physica status solidi (a)

Check for updates

RESEARCH ARTICLE OPEN ACCESS

Structural Tailoring of Polyaniline Synthesized by Acid-Assisted Polymerization at Room Temperature: Insights Into Polaron Dynamics

Stephen Boahene[1,2,3] | Štěpán Potocký[1,2] | Kateřina Aubrechtová Dragounová[2,4] | Elena Tomšík[5] | Alexander Kromka[2]

[1]Faculty of Electrical Engineering, Czech Technical University in Prague, Technická, Czech Republic | [2]Institute of Physics, Czech Academy of Sciences, Prague, Czech Republic | [3]Faculty of Science & Technology, Hasselt University, Hasselt, Belgium | [4]Faculty of Nuclear Sciences and Physical Engineering, Czech Technical University in Prague, Prague, Czech Republic | [5]Institute of Macromolecular Chemistry, Czech Academy of Sciences, Prague, Czech Republic

Correspondence: Stephen Boahene (boaheste@fel.cvut.cz)

Received: 27 May 2025 | **Revised:** 8 October 2025

Keywords: acid-assisted polymerization | photoluminescence (PL) measurement | polyaniline | Raman measurement

ABSTRACT

This work presents a detailed study of the synthesis and characterization of polyaniline (PANI) using a novel acid-assisted polymerization method with varying ammonium persulfate concentrations. Two distinct PANI samples were synthesized at room temperature, resulting in different morphologies. Scanning electron microscopy revealed a porous nanofibrillar morphology for PANI1, while PANI2 exhibited a densely packed morphology. Raman spectroscopy confirmed the presence of semiquinoid units, with characteristic bands at ~1602 and ~1500 cm^{-1} in both PANIs. UV–Vis spectroscopy revealed characteristic absorption bands at 259 and 428 nm, attributed to π–π^* transitions and localized polarons transitions, respectively. Photoluminescence measurements identified emission bands at 2.26 and 2.18 eV, further supporting the presence of π–π^* transitions. The observed energies suggest a mechanism involving the electron transfer coupled with reorganization energy, contributing to the observed spectral features. Fourier transform infrared spectroscopy confirmed the presence of key functional groups, including C—H bending vibrations at ~1140 cm^{-1}. Given that PANI is a p-type semiconductor with holes as the majority charge carriers, this work provides valuable insights into the structure–property relations of PANI synthesized via this novel synthesis method. These findings seem promising for the integration of PANI with carbon-based materials, forming a composite system (electrode) for advanced energy storage applications.

1 | Introduction

An important factor in the deployment of electroactive materials for energy storage systems is the ability to control and tailor their properties and characteristics [1]. These energy storage systems include fuel cells, batteries, and electrochemical capacitors. Fuel cells and batteries exhibit a high density, which renders them appropriate for applications requiring a sustained power supply, such as electric vehicles and portable electronic devices that require perennial power [1–3].

However, the demand for electrochemical capacitors, also known as supercapacitors, has increased due to quicker charging and discharging properties and higher energy density [1, 3]. Polyaniline (PANI) has garnered considerable scientific interest following the discovery of conducting polymers. It has been notably highlighted for its diverse potential applications (e.g., gas sensors, catalysis, composite fabrication, and adsorption) and notable advantages, encompassing facile synthesis, cost-effectiveness, robust environmental stability, and exceptional performance attributes [4]. There is a growing demand for conjugated polymers with specific

This is an open access article under the terms of the Creative Commons Attribution License, which permits use, distribution and reproduction in any medium, provided the original work is properly cited.

© 2025 The Author(s). *physica status solidi (a)* applications and materials science published by Wiley-VCH GmbH.

morphologies and properties required for particular device applications [1]. Consequently, a reliable, simple, and dependable synthesis is needed.

Semiconducting polymers are currently produced using a variety of techniques, including chemical oxidation polymerization [5], typically carried out using strong acids (e.g., HCl), but can also employ aromatic and carboxylic acids as dopants during synthesis [6], electrochemical polymerization [7], metal-catalyzed coupling [8], solid-state polymerization [9], Lewis acid-assisted polymerization [10], acid-assisted polymerization [1, 11], photo-induced polymerization, and high-temperature oxidant-free acid polymerization [12]. PANI synthesis is highly dependent on several factors that affect aniline polymerization conditions, such as oxidant, solvent, electrode material, pH, temperature, and presence of chemical additives (like oligoaniline and π-bonding compounds), as well as the composition of the electrolyte and dopant anions [13]. The influence of these factors on PANI synthesis subtly modulates the PANI molecular structures and characteristics. To achieve desired physicochemical properties that can help enhance performance in various applications, it is necessary to optimize the polymerization parameters. The primary approach for producing PANI with controlled size and morphology is chemical oxidative polymerization, which has enormous promise for technological synthesis applications. However, a significant challenge in this area is the frequent formation of insoluble PANI suspensions, which negatively impacts the interfacial conductivity in composite electrode materials. This issue has led to considerable scientific interest in developing stable PANI suspensions via solution methods, particularly in formic acid [11, 14–16]. Recent work by Trchová et al. investigated PANI prepared in formic acid solutions, focusing on functionalization with carboxyl groups. Their spectroscopic analyses indicated ring carboxylation when PANI was synthesized with a stoichiometric peroxydisulfate-to-aniline mole ratio in formic acid solutions, yielding results comparable to those obtained for aniline oxidation in other carboxylic acids [14]. However, despite these promising findings, challenges arose with homogeneous polymerization at higher anthranilic acid concentrations due to its poor water solubility, leading to heterogeneous syntheses and the potential for unreacted anthranilic acid [14]. Nevertheless, novel protocols have emerged where PANI is synthesized at room temperature for fabricating sensing layers using PANI films and chelating agents [11] and for enhancing the electrochemical performance of diamond electrodes [1].

PANI, a representative conducting polymer, can exhibit three principal oxidation states determined by the ratio of imine (–N=) to amine (–NH–) nitrogen functionalities within the polymer backbone. The fully oxidized state is designated pernigraniline, while the fully reduced state is leucoemeraldine. Intermediate oxidation levels correspond to the emeraldine [17]. The emeraldine base form of PANI is typically insulating. Protonation (doping) of emeraldine base with an acid generates the emeraldine salt (ES) form, which exhibits significantly enhanced electrical conductivity and represents the most conductive state [17]. Conversely, treatment with base causes dedoping, reverting the polymer to the emeraldine base form. The molecular structure of PANI, highlighting the alternating benzenoid and quinoid units that constitute its conjugated polymer backbone, can be seen in Figure 1. The electrical conductivity of PANI is strongly dependent on the doping level, spanning a

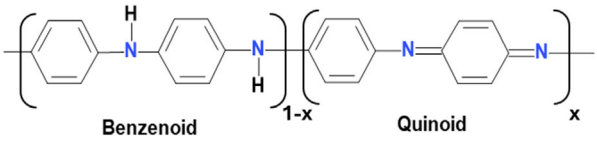

FIGURE 1 | The molecular structure of PANI illustrating the benzenoid and quinoid units along the polymer backbone.

range typically from 10^{-10} to 10^{-1} S/cm [17, 18]. The electrical conductivity of PANI films is primarily governed by the oxidation state, the pH of the electrolyte (in electrochemical environments), and the specific dopant employed for protonation [17].

Electronic level energies are critical parameters for characterizing materials utilized in organic electronics. These parameters include the energy of ionized levels or the levels allowed for excess holes and electrons (HUMO and LUMO levels, respectively), which are crucial factors in determining the heights of metal–organic interfaces and interface barriers in multicomponent structures (organic solar cells, organic light-emitting diodes, etc.); as a result, it is imperative to determine these levels accurately. Techniques such as ultraviolet photoelectron spectroscopy and inverse photoelectron spectroscopy allow direct probing of the HOMO and LUMO levels, respectively [19–22].

Understanding the structure–property relationships in conducting polymers to form heterostructures with other composite materials is vital for the advanced of next-generation technologies. These include field-effect transistors, organic light-emitting diodes, plastic transistors and logic gates, photovoltaic cells, antistatic coatings [23], and electrochemical capacitors [1].

This study investigates the physical-chemical characteristic properties of PANI, with particular emphasis on the sequence of elementary steps/reactions during its oxidative polymerization and the corresponding photoluminescence (PL) behavior of the resulting materials.

A facile synthesis protocol for PANI was achieved at room temperature through oxidative polymerization of aniline, a weak base, utilizing ammonium persulfate (APS) as an initiator and formic acid as both the reaction medium and a potential doping agent. This unique approach distinguishes itself by its operational simplicity, achieved by not requiring a specialized reaction apparatus, which facilitates accessible PANI production. While polymerization at 0°C [24] is the most common approach perpetuated in a few studies, synthesis at ambient temperature (approximately 25°C) has also been extensively demonstrated. This work maintained temperature control by placing the reaction vessel in an insulated container to minimize heat exchange with the surroundings. Simultaneously, a water bath was maintained at 25°C to stabilize the reaction environment [25].

Compared with earlier studies, our approach introduces several methodological distinctions. In contrast to protocols using strong mineral acids such as hydrochloric acid [26], the present synthesis employs concentrated formic acid as both medium and potential dopants. While prior work using formic acid [14] achieved successful polymerization, our method incorporates ethanol as a cosolvent to enhance dissolution of any partially insoluble

18626319, 0, Downloaded from https://onlinelibrary.wiley.com/doi/10.1002/pssa.202500433 by Universiteit Hasselt Dienst Financiën, Wiley Online Library on [05/01/2026]. See the Terms and Conditions (https://onlinelibrary.wiley.com/terms-and-conditions) on Wiley Online Library for rules of use; OA articles are governed by the applicable Creative Commons License

intermediates, thereby promoting a more homogeneous and controlled reaction. Furthermore, relative to our group's earlier report on PANI synthesis [15], the present study expands the scope of characterization and focuses on detailed analysis of polaronic dynamics after polymerization. These refinements allow for deeper insight into the structure–property relationships of the resulting PANI materials.

2 | Results and Discussion

2.1 | Synthesis of Polyaniline (PANI1 and PANI2)

This study reports the synthesis of PANI via the oxidative polymerization of aniline in concentrated formic acid at room temperature (Figure 2). Under these conditions, formic acid dissociation reduces aniline monomer's protonation, thereby minimizing its influence on the charge transfer between aniline and the initiator (APS). The stabilization of charged intermediates formed during the electron transfer between the aniline monomer comes as a result of concentrated formic acid acting as a polar protic solvent. This stabilization, however, modulates the reaction kinetics. The reason for this is that formic acid can solvate and stabilize the charged species, like radical cations, that are formed during electron transfer. This, however, can lower the activation energy of the reaction and affect the reaction rate, k. The progression of the polymerization is indicated by the formation of a solution with a dark green hue (reacted solution, see Figure 3), confirming the saturation of PANI synthesis.

Figure 3 presents the color evolution of PANI1 and PANI2 reaction mixtures over time. These changes are observed by monitoring the colorimetric response performed at 5-min intervals and are a result of the aniline to ammonium persulfate (APS) ratio's reaction kinetics. Despite being referred to as an oxidant in the case of a semiconducting polymer, APS works as an initiator in this particular reaction. A fundamental step within the polymerization mechanism is the generation of cation radicals, which are active in electron transfer.

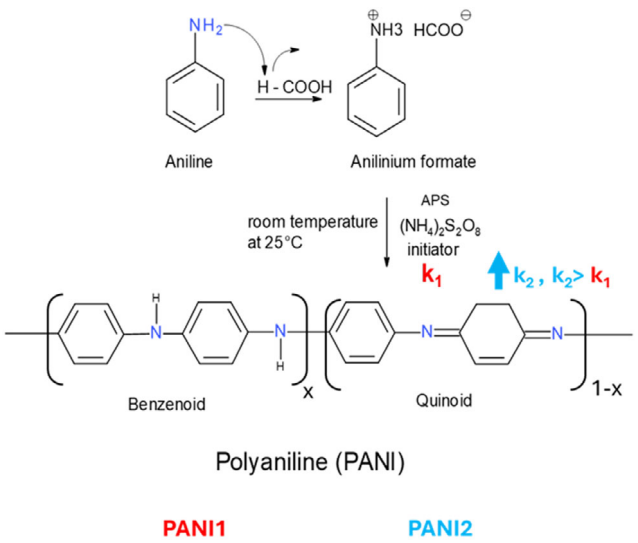

FIGURE 2 | Schematic illustration of acid-assisted polymerization of aniline monomer in the presence of concentrated formic acid and upon the addition of an initiator (APS) into PANI suspensions.

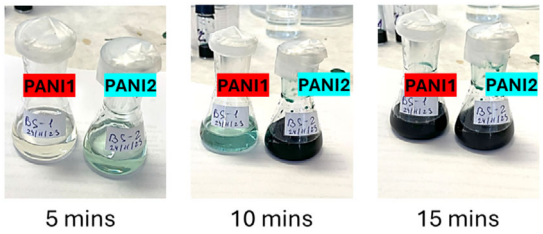

FIGURE 3 | Illustration of the time-dependent reaction dynamics during the polymerization of PANI1 and PANI2 with different aniline: APS ratios.

PANI2 exhibits a fast turquoise coloration within 5 min, suggesting an early stage of rapid polymerization, whereas PANI1 remained initially colorless. After 10 min, PANI2 progressed to a dark green hue, while PANI1 showed turquoise, indicating delayed polymerization. The colorimetric difference suggests that PANI2 had advanced beyond initiation and into propagation and potentially saturation, while PANI1 was still in the early stage of polymerization. By 15 min, both solutions exhibited the characteristic dark green hue, indicating that the reaction had reached saturation under the given conditions. These temporal colorimetric changes qualitatively reflect the progression through initiation and propagation, with eventual saturation corresponding to initiator/monomer depletion and stabilization of the ES phase. The polyaniline suspensions were harvested immediately after the 15-min mark to suppress further polymerization.

2.2 | UV–Vis Spectrum Measurement of PANI1 and PANI2

Figure 4 shows the UV–Vis measurement of PANI1 and PANI2 recorded over the range 190–800 nm. Three characteristic bands can be identified: a prominent absorption band at 259 nm may correspond to a π–π^* electronic transition of the benzenoid rings within the polymer backbone, consistent with recent findings by Bláha et al. [27], who assigned a similar absorbance band around 270 nm to this transition. The second band observed at 428 nm in the visible region is attributed to the localized polaron transitions [27] and to the C = N group in protonated imine structures, associated with benzenoid units and nitrogen lone pair interactions [28], which originates from the protonation (via its dissociation)

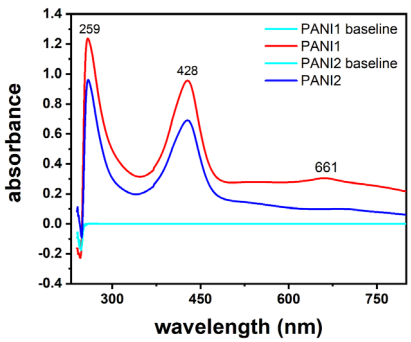

FIGURE 4 | UV–Vis absorption spectra of PANI1 and PANI2.

18626319, 0, Downloaded from https://onlinelibrary.wiley.com/doi/10.1002/pssa.202500433 by Universiteit Hasselt Dienst Financiën, Wiley Online Library on [05/01/2026]. See the Terms and Conditions (https://onlinelibrary.wiley.com/terms-and-conditions) on Wiley Online Library for rules of use; OA articles are governed by the applicable Creative Commons License

process facilitated by HCOOH. This process converts the insulating leucoemeraldine base into the conductive ES and simultaneously promotes the formation of a more ordered molecular structure. The absorption observed at 661 nm is characteristic of the emeraldine base form of PANI, corresponding to the excitonic transition between its quinoid and benzenoid units [29]. Upon acid doping, the emeraldine base converts to the ES, resulting in a pronounced decrease in the intensity of the 661 nm absorption band, a phenomenon known as hypochromism [29] which is attributed to alterations in the quinoid units, consistent with conformational changes such as the adoption of a random coil configuration in the PANI salt form [29] leading to increased agglomeration [30]. Notably, PANI2 exhibited a more pronounced hypochromic shift than PANI1, correlating with different polymerization times, as illustrated in Figure 3. The prominence of these benzenoid unit-related bands confirms the expected chemical structure of the synthesized PANI.

2.3 | Fourier Transform Infrared Measurement of PANI1 and PANI2

The Fourier transform infrared (FTIR) spectra of PANI synthesized via acid-assisted method are shown in Figure 5. Both samples exhibited similar spectral features, regardless of their morphological differences. Bands at 1498 and 1533 cm^{-1} correspond to the vibrations of benzenoid and quinoid rings, respectively [14]. These bands can be a result of the influence of the formic acid on the chemical structure and bonding of PANI. The shifts in the C = C and C = N ring stretching frequencies suggest electron density changes and bond order of the benzenoid and quinoid rings, respectively. However, this can result from the protonation of the polymer backbone by the formic acid, which can lead to the delocalization of charges and changes in structures. Additionally, the in-plane bending vibrations of C—H bonds associated with protonated nitrogen atoms, i.e., N = Q = N, Q = NH^+—B, and B—NH^+ functionalities, where Q represents the quinoid ring and B represents the benzenoid ring, can be observed at the band 1140 cm^{-1} [31, 32]. The vibration band around ~1140 cm^{-1}, often referred to as the electron-like band or polaron band, is strongly associated with the delocalized polaronic structure in doped PANI (ES) [33]. This band originates from the protonation process during synthesis and is assigned to C—H in-plane bending coupled with the stretching of quinoid and benzenoid rings, becoming enhanced in the doped state, due to charge delocalization along the polymer backbone [34].

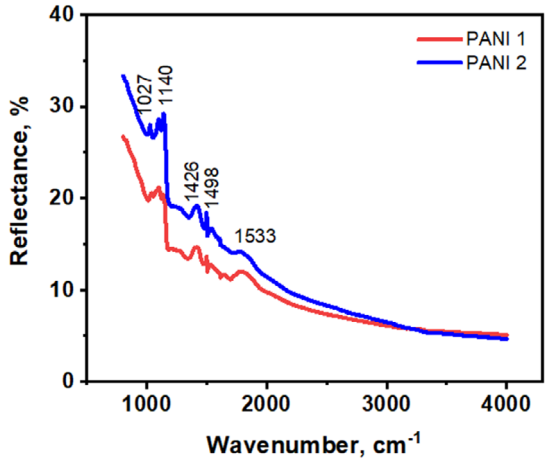

FIGURE 5 | FTIR spectra of PANI1 and PANI2 synthesized via an acid-assisted polymerization method.

2.4 | X-Ray Diffraction Analysis of PANI1 and PANI2

X-ray diffraction (XRD) was employed to elucidate the crystal structure, degree of crystallinity, and average crystallite size of the synthesized PANI suspensions, as these parameters strongly affect the electronic performance of conducting polymers. The diffraction patterns (Figure 6) confirm that both PANI1 and PANI2 adopt an orthorhombic lattice, characterized by $\alpha = \beta = \gamma = 90°$ [35, 36]. A comparison of the diffraction peak profiles reveals that PANI1 exhibits sharper and more intense reflections, consistent with a higher degree of crystallinity. In contrast, PANI2 shows broader reflections with larger full width at half maximum (FWHM) values (see Tables 1 and 2), indicative of smaller crystallite sizes and reduced crystallinity. These parameters strongly affect the electronic performance of the synthesized PANI suspensions.

Quantitatively, the relative peak intensities further highlight the influence of the aniline:APS ratio on the crystalline features. At ~6.1° 2θ, the intensity of PANI1 is approximately 1.6 times greater than that of PANI2. At ~18.3° 2θ, the difference becomes more pronounced, with PANI1 exhibiting nearly threefold higher intensity. In contrast, PANI2 shows stronger diffraction peaks at ~20.5° and ~29.3° 2θ, where the intensities are ~1.8 and ~1 times higher than those of PANI1. These systematic variations suggest that a higher aniline: APS ratio in PANI1 favors the development of long-range interchain order, whereas the relatively higher APS content in PANI2 promotes localized ordering along the polymer backbone at higher diffraction angles.

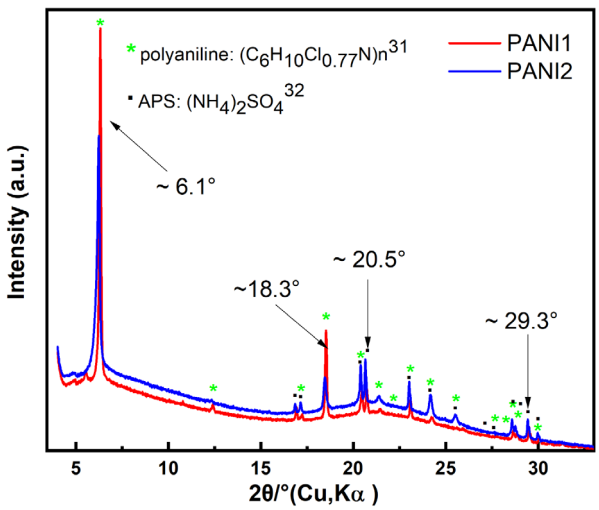

FIGURE 6 | XRD patterns of PANI1 and PANI2. Selected reflections corresponding to polyaniline and residual APS are indicated. Sharper peaks for PANI1 confirm higher crystallinity, whereas broader peaks for PANI2 indicate reduced crystallinity.

18626319, 0, Downloaded from https://onlinelibrary.wiley.com/doi/10.1002/pssa.202500433 by Universiteit Hasselt Dienst Financiën, Wiley Online Library on [05/01/2026]. See the Terms and Conditions (https://onlinelibrary.wiley.com/terms-and-conditions) on Wiley Online Library for rules of use; OA articles are governed by the applicable Creative Commons License

TABLE 1 | The refined unit cell parameters of PANI1 obtained from XRD analysis.

Position [° 2θ]	d-spacing [Å]	Height [cts]	FWHM [°2θ]
~6.1(8)	14.21854	66 333.46	0.0985(3)
~18.3(2)	4.8152	18 931.21	0.0909(9)
~20.5(6)	4.30462	5684.4	0.077(3)
~29.3(9)	3.03592	3622.8	0.079(3)

TABLE 2 | The refined unit cell parameters of PANI2 obtained from XRD analysis.

Position [° 2θ]	d-spacing [Å]	Height [cts]	FWHM [°2θ]
~6.1(2)	14.48065	40 592.52	0.1737(7)
~18.3(6)	4.83257	6329.41	0.143(3)
~20.5(4)	4.3211	10 275.54	0.065(1)
~29.3(6)	3.04364	4807.51	0.070(2)

2.5 | Raman Measurement of PANI1 and PANI2

The Raman spectra of aniline, PANI1, and PANI2 are shown in Figure 7. The excitation wavelength employed for this measurement was 785 nm due to the greater sensitivity to phases contained and PL elimination. The Raman spectrum of aniline exhibited characteristic vibrational bands, providing insights into its molecular structure [37, 38]. Prominent bands at 1405 and 1709 cm^{-1} were observed and attributed to in-plane C—C stretching vibrations of the aromatic ring. The band at 1211 cm^{-1} was assigned to C—N stretching mode of the amino group attached to the aromatic ring [37]. Less intense bands were also detected at approximately 2964 and 702 cm^{-1}, corresponding to aromatic C—H stretching vibrations [38] and in-plane N—H bending, respectively [39]. PANI1 and PANI2 revealed very similar spectral features. Key features included bands at 1600 and 1500 cm^{-1} corresponding to C—C stretching in semiquinoid rings, the —C=N— stretching vibrations, and C = C stretching of imine, respectively [1, 16]. Furthermore, characteristic vibrational bands for the emeraldine base form of polyaniline were observed: an out-of-plane ring deformation mode at approximately 516 cm^{-1} [40–42] and an in-plane C—H bending mode of quinoid units at around 1180 cm^{-1} [40].

2.6 | Scanning Electron Microscopy and Transmission Electron Microscopy Measurement of PANI1 and PANI2

Surface morphological analysis presented in Figure 8 reveals distinct differences between the PANI1 and PANI2 suspensions. The polymerization kinetics of PANI1 are slower than those of PANI2, as corroborated by its delayed color change in Figure 3. In contrast, the accelerated polymerization of PANI2 leads to a less ordered nano-object morphology, as seen in Figure 8c,d. Consequently, distinct electrochemical performances are anticipated for PANI1 and PANI2 [1]. The scanning electron microscopy (SEM) images in Figure 8a,b of PANI1 films revealed consistent porous and nanofibril-like features, respectively. Conversely, PANI2 films exhibit a dense and less porous morphology. Complementary to the SEM images, transmission electron microscopy (TEM) micrographs of the synthesized polyaniline (PANI) samples are shown in Figure 8e,f, also revealing distinct morphological features as a function of the aniline:APS molar ratio employed during polymerization. Specifically, PANI1 exhibits sparsely distributed, loosely entangled polymer chains, while for PANI2, the morphologies exhibit dense entanglement, resulting in polymers being compacted into aggregates. The synthesis was repeated three times, yielding consistent morphological and spectroscopic results (Figures S1 and S2). Observed morphological differences between PANI1 and PANI2 are linked to the kinetics of polymerization. The formation of a

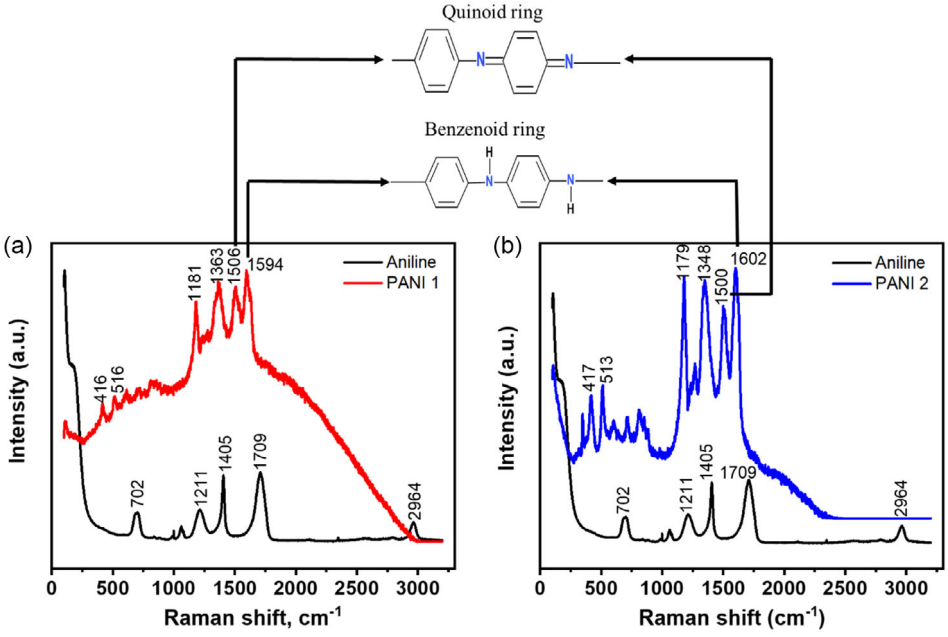

FIGURE 7 | Raman spectra of (a) aniline and PANI1 and (b) aniline and PANI2, measured with the 785-nm excitation wavelength.

18626319, 0, Downloaded from https://onlinelibrary.wiley.com/doi/10.1002/pssa.202500433 by Universiteit Hasselt Dienst Financiën, Wiley Online Library on [05/01/2026]. See the Terms and Conditions (https://onlinelibrary.wiley.com/terms-and-conditions) on Wiley Online Library for rules of use; OA articles are governed by the applicable Creative Commons License

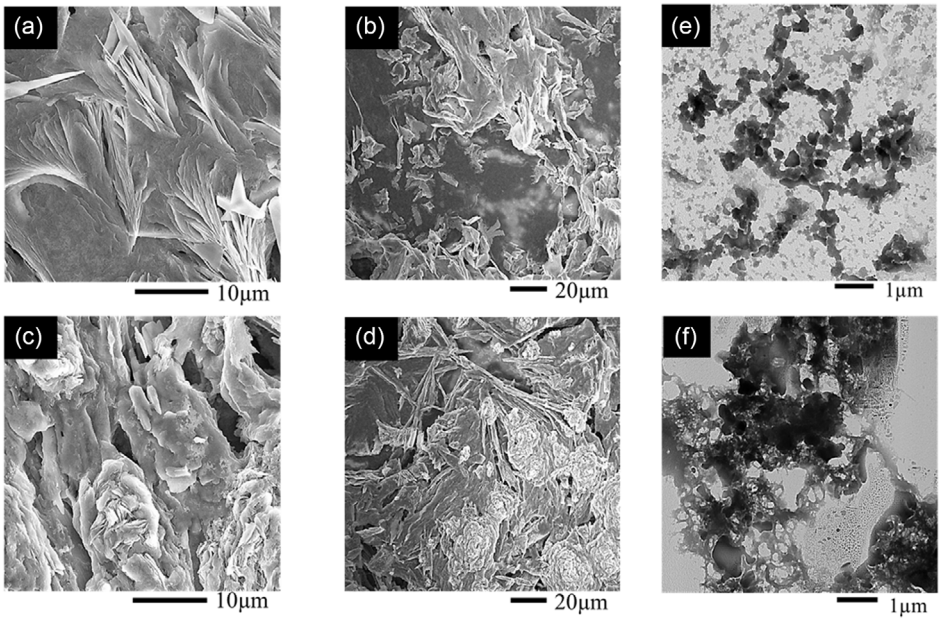

FIGURE 8 | SEM images of PANI1 at (a) low and (b) high magnification and PANI2 at (c) low and (d) high magnification, both PANI deposited on Au substrates, and TEM images of (e) PANI1 and (f) PANI2 at 1 μm scale.

well-ordered PANI network architecture is likely to be hindered by the rapid polymerization process in the case of PANI2, in contrast to PANI1, where slower kinetics can be observed, suggesting that controlled polymerization kinetics can promote the formation of well-defined polymer structures, which could consequently influence the performance of composite materials incorporating such PANI architectures [1]. While Raman spectroscopy revealed comparable benzenoid and semiquinoid contributions in both PANI1 and PANI2, the SEM images of PANI1 and PANI2 differed significantly. We hypothesized that the variations in aniline:APS ratios employed for the synthesis led to differences in the kinetics of polymerization, which dominated the morphological variations observed. Specifically, a higher aniline:APS ratio promoted slower nucleation and growth, leading to smaller particle sizes and porous structures. A lower aniline:APS ratio showed faster nucleation and growth, leading to higher particle sizes and densely packed structures, which affected the branching/cross-linking of the polymer chains.

2.7 | PL Measurement of PANI1 and PANI2

The PL spectra (Figure 9) provide insights into the electronic transitions between the highest energy occupied molecular orbital (HOMO) and the lowest energy unoccupied molecular orbital (LUMO) [43]. The PL in PANI was postulated to be visible if the reduced benzenoid units and oxidized quinoid units formed a phase-separated structure [43, 44]. Additionally, the PL requires more than two benzenoid units that are not next to a quinoid unit [44]. PANI1 exhibits broad bands at 548 nm (2.26 eV), 596 nm (2.08 eV), and 712 nm (1.74 eV), and PANI2 exhibits bands at 568 nm (2.18 eV) and 696 nm (1.78 eV). Bands at 548 and 568 nm for PANI1 and PANI2, respectively, are likely due to the π–π^* transitions [19]. The band positions and their transition assignment are summarized in Table 3. The transitions responsible for NIR broad bands are not clear to the best of our knowledge. The presence and different numbers of observed bands mainly suggest different HOMO–LUMO gaps in the two PANI samples. Moreover, the gaps are crucial to the material's optoelectronic property determination [19]. A smaller HOMO–LUMO gap facilitates easie Moreover, the gaps are crucial in determining the material's optoelectronic properties [19]. A smaller HOMO–LUMO gap facilitates easier electron movement, leading to higher conductivity of the material. In conjugated systems, the π orbitals overlap, leading to electron delocalization, which reduces the HOMO–LUMO energy gap and thus shifts π–π^* transitions to lower energies (longer wavelength) [45]. The PL intensity depends on the reorganization energy due to the electron transfer during the synthesis, as postulated by Marcus theory [46, 47]. This delocalization decreases the HOMO–LUMO energy gap with shifts π–π^* transitions toward lower energies (longer wavelengths) [45].

It is worth noting that the weak absorption observed at 661 nm in the UV–Vis spectrum and the low PL intensity in this region indicate that no effective radiative energy transfer takes place here, i.e., that there is a low probability of emission transitions. This is consistent with the low oscillator strength of the related transition.

2.8 | Discussion

Kohut et al. [16]. recently investigated the nonconducting polyaniline nanofibrils and their physicochemical behavior, including their PL spectra recorded at 442 and 785 nm excitation wavelengths after alkali treatment. In our current study, we compare the PL response of our synthesized PANI samples, obtained using a 442 nm excitation wavelength, with their results. Under the same excitation (at 442 nm), Kohut et al. observed prominent PL wavelengths at approximately 550, 582, and 1100 nm.

18626319, 0, Downloaded from https://onlinelibrary.wiley.com/doi/10.1002/pssa.202500433 by Universiteit Hasselt Dienst Financiën, Wiley Online Library on [05/01/2026]. See the Terms and Conditions (https://onlinelibrary.wiley.com/terms-and-conditions) on Wiley Online Library for rules of use; OA articles are governed by the applicable Creative Commons License

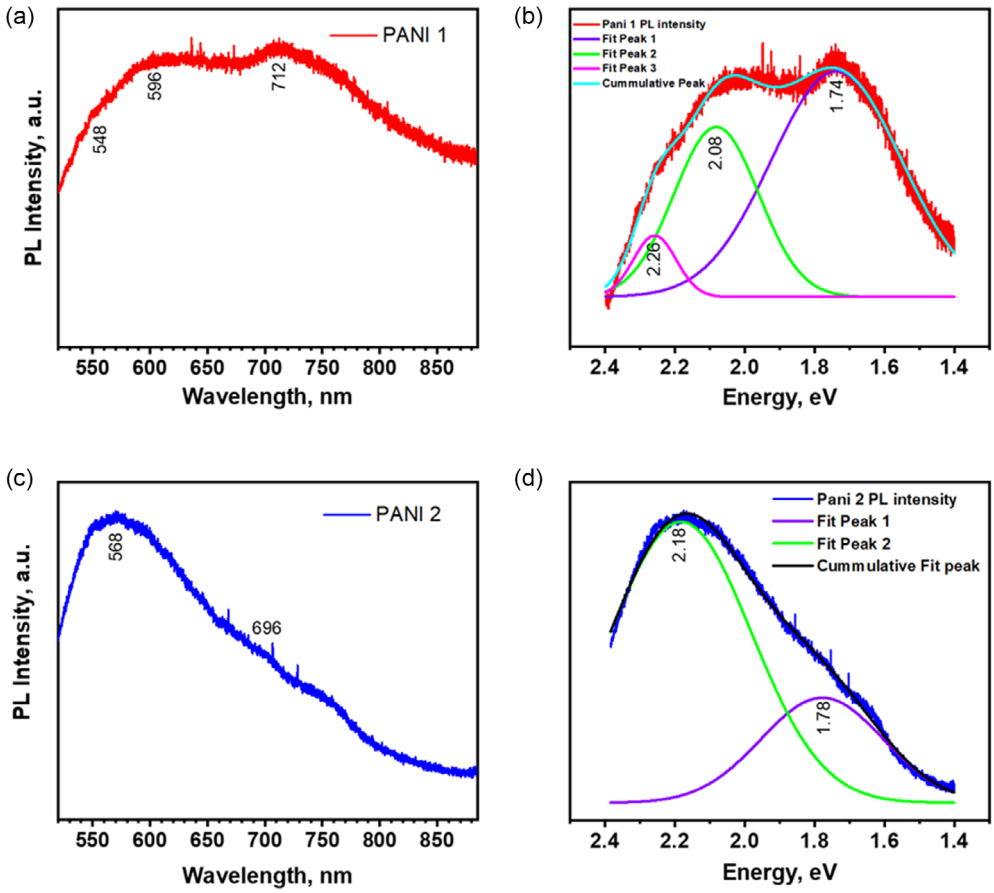

FIGURE 9 | PL spectra of (a) PANI1 with (b) its fitted Gaussian bands in energy scale and (c) PANI2 with (d) its fitted Gaussian bands, irradiated by the excitation wavelength of 442 nm.

TABLE 3 | Summary of the PL bands and their assignment for PANI1 and PANI2.

Sample	Wavelength (λ) [nm]	Energy [eV]	Assignment
PANI1	548	2.26	π–π^* transitions suggesting HOMO–LUMO gaps [19]
	596	2.08	π–π^* transitions, polaron–bipolaron transitions suggest a radiative recombination process occurring within the PANI structure [48]
	712	1.74	
PANI2	568	2.18	π–π^* transitions suggesting HOMO–LUMO gaps [19]
	696	1.78	

The wavelength at 550 nm corresponds to a higher-energy transition (2.25 eV), while that of 1100 nm is associated with a lower-energy transition (1.12 eV). Their observations revealed similarities in the intensities of both main peaks (550 and 1100 nm), and the emission at 1100 nm is twice as high as the emission at 550 nm. However, their intriguing observation is explained by the proximity of the 442 nm excitation wavelength to the bandgap, which may induce second harmonic PL [16] that is predominantly observed in crystalline inorganic semi-insulating materials [16, 49].

By comparison, the PL spectra of PANI1 and PANI2 (Figure 9), measured at the same excitation wavelength, exhibit higher-energy transitions. Deconvolution using Gaussian band fitting reveals distinct emission transitions, providing a more resolved understanding of the underlying photophysical processes.

The higher transition energies observed in our samples, relative to those reported by Kohut et al. [16], can be attributed to differences in electron reorganization energy during the charge–transfer processes. In their investigation, one key component reflected in the low photon energy band around 1100 nm was a result of the chemical structure and PANI nanofibrils' morphology. This absorbed energy does not dissipate into vibrational or rotational energies because the benzenoid ring in the nanofibrils is rigid [16]. Contrary to the prior report, our current study did not show an

18626319, 0, Downloaded from https://onlinelibrary.wiley.com/doi/10.1002/pssa.202500433 by Universiteit Hasselt Dienst Financiën, Wiley Online Library on [05/01/2026]. See the Terms and Conditions (https://onlinelibrary.wiley.com/terms-and-conditions) on Wiley Online Library for rules of use; OA articles are governed by the applicable Creative Commons License

energy band around 1100 nm, as this significant difference is attributed to the unique sample preparation technique implemented, highlighting its critical influence on the observed electronic characteristics of PANI.

The XRD analysis further supports the structural differences between PANI1 and PANI2. The sharper and more intense reflections observed for PANI1 indicate a higher degree of crystallinity, whereas the broader peaks and larger FWHM values in PANI2 confirm reduced crystallinity and smaller crystallite domains. These results are consistent with the SEM/TEM observations, where the slower polymerization kinetics of PANI1 favored the development of ordered nanofibrillar networks, while the accelerated kinetics of PANI2 led to a more compact and partially amorphous morphology. These findings highlight that the aniline:APS ratio not only dictates the morphology but also strongly influences the crystalline order of PANI, with direct implications for charge transport and overall electronic performance.

Particularly, the PL emission characteristics are critically influenced by the polaronic dynamics, which in turn are governed by the charge–transfer kinetics during polymerization. These dynamics are strongly dependent on both the chemical structure and morphology of the PANI nanostructures. The combined results from Raman and PL spectroscopy and XRD measurements confirm that the electronic properties of PANI can be systematically tuned through precise control of the synthesis conditions.

The acid-assisted polymerization method of aniline developed in this work enables the synthesis of PANI without requiring specialized reaction apparatus. This novel method yielded stable, thick-layered PANI suspensions, unlike the traditional techniques that typically result in precipitation of PANI suspensions that are insoluble due to the inherent stiffness of the PANI backbone and heavily conjugated π electron configuration [50, 51]. Furthermore, this method facilitates control over the polymerization kinetics, allowing the formation of concentrated, stable dispersions rather than thin films typically observed in other protocols [51]. The ability to produce stable, thick-layered PANI-based suspensions at room temperature represents a significant advancement, offering new opportunities for tailoring PANI-based composites in supercapacitors [1, 15] and optoelectronic [52] applications.

These findings indicate the need for further optimization of the acid-assisted polymerization of PANI. We hypothesized that controlling the reaction kinetics, particularly by reducing the initiator concentration, is a critical parameter for improving the polymer morphology. To validate this, future work will involve a systematic study of the initiator concentration effects on both the reaction kinetics and the resulting PANI morphology. Furthermore, a comprehensive time-dependent study is planned to evaluate the long-term stability and lifespan of the PANI suspensions. Altogether, it will provide essential information for their proposed applications. In addition to reaction kinetic optimization, variability in morphology between batches, even under nominally identical conditions, remains an important factor for further study. Moreover, the scalability of the formic acid-assisted polymerization method to larger production volumes has not yet been systematically evaluated. Addressing these aspects will be essential for translating this synthesis protocol into practical, industrial-scale applications.

3 | Conclusion

The successful establishment of PANI synthesis via acid-assisted polymerization technique in the presence of a monomer (aniline) was demonstrated. Stable PANI suspensions were formed by reducing the concentration of the initiator (APS) through acid-assisted polymerization synthesis, highlighting the effectiveness of acid-assisted polymerization in controlling the reaction environment. Two different precursor ratios were explored: PANI1 (aniline:APS = 10:1) and PANI2 (aniline:APS = 5:1).

PANI1 produced smaller nanofibrils and exhibited less densely packed structures compared to PANI2. PL measurements revealed that PANI1 exhibited higher photon energy emission, likely due to its less conductive, more isolated structure.

Conversely, PANI2 formed more densely packed and conductive structures, but its limited interaction with electrode surfaces may reduce its suitability for energy-storage applications [1]. The polymerization kinetics followed a classical three-step mechanism—initiation, propagation, and saturation—which was qualitatively tracked via observable color changes during the reaction. PANI2 polymerized within 10 min, while PANI1 required 15 min, indicating a difference in reaction rates attributed to the varying initiator concentrations.

Morphological analysis using SEM confirmed the formation of porous nanofibril-like structures in PANI1 and more compact, densely packed structures in PANI2. Raman measurement identified characteristic vibrational modes corresponding to benzenoid and semiquinoid units, confirming their presence in the molecular structure.

As luminescence is a distinctive feature of aromatic systems, its observation clearly proves that structural patterns exist. The influence of the insights on the polaron dynamics of PANI due to electron transfer during synthesis comes as a result of the relative intensity of the bands, which depends on the reorganization energy. Furthermore, the π–π^* transitions were observed at lower energies, consistent with a reduced HUMO–LUMO energy gap due to the π orbitals' overlap and increased electron delocalization. Overall, the results demonstrate that precise control over synthesis parameters enables tuning of the structural, electrical, and optical properties of PANI, paving the way for optimized materials for future energy-storage and optoelectronic applications. In addition, XRD analysis revealed that the aniline:APS ratio governs the crystalline order of PANI, with PANI1 exhibiting enhanced long-range order and PANI2 showing reduced crystallinity and partial lattice distortion, further linking synthesis stoichiometry to electronic performance.

4 | Experimental Section/Methods

4.1 | Materials

Analytical grade aniline,ammonium persulfate (APS) (99% Lachner, Czech Republic), concentrated formic acid (98% Sigma–Aldrich, Czech Republic), orthophosphoric acid (85%, Merck,

18626319, 0, Downloaded from https://onlinelibrary.wiley.com/doi/10.1002/pssa.202500433 by Universiteit Hasselt Dienst Financiën, Wiley Online Library on [05/01/2026]. See the Terms and Conditions (https://onlinelibrary.wiley.com/terms-and-conditions) on Wiley Online Library for rules of use; OA articles are governed by the applicable Creative Commons License

Czech Republic), and ethanol (99.8%, Sigma–Aldrich, Czech Republic) were used.

4.2 | Synthesis of Polyaniline (PANI)

Synthesis of PANI1 and PANI2: PANI was synthesized by a novel method of acid-assisted polymerization at room temperature (25°C) [1]. A 0.3 M aniline solution (0.2 ml) was dissolved in 1 ml of ethanol and 4.7 ml of concentrated formic acid. The resulting solution was mixed with 0.03 M (0.047 g) of ammonium persulfate (APS dissolved in 1 ml of distilled water). Polymerization was initiated by the rapid addition of an aqueous ammonium persulfate (APS) solution. The solution was labeled as PANI1 (aniline: APS molar ratio = 10:1). For PANI2, the APS concentration was doubled (0.094 g in 1 mL of deionized water), resulting in an aniline:APS molar ratio of 5:1. The increased APS concentration in the PANI2 synthesis led to a demonstrably faster polymerization rate [1].

4.3 | Material Characterization

Absorbance spectra of PANI1 and PANI2 were measured using a Jasco V 730 spectrometer in the range of 190–800 nm in a quartz cuvette (Hellma 105-10-40) with a 10 mm light path. The model's wavelength measurement accuracy is ±0.2 nm (656.1 nm). Sample preparation was done by using deionized water as the solvent during the UV–Vis measurement, as dispersed polyaniline solutions were prepared in a ratio of 1:1000.

FTIR spectroscopy was employed to investigate the functional groups of the polymer using a Nicolet IS50 FTIR spectrometer (Thermo Fisher Scientific Inc.), with a KBr beam splitter and N_2-cooled MCT-HighD detector. All spectra were measured using the specular apertured grazing angle reflectance method. Each spectrum represents an average of 128 scans per spectrum collected in the range of 4000–800 cm^{-1}. A bare Au substrate was measured as a background prior to each sample measurement. Baseline correction was performed on all measured spectra.

Raman and PL spectra of PANI-dried droplets were collected in reflecting geometry using Renishaw in Via Reflex Raman microscope (Renishaw, UK) with a Peltier-cooled CCD detector. For Raman measurements, a 785-nm excitation laser line (Renishaw HPNIR785 laser source) was used, while 442-nm line of HeCd laser (Kimmon Koha) was used for PL measurement. In confocal mode, the Leica objectives (100x with NA = 0.9 and 50x LWD with NA = 0.5) were used to gather scattered and emitted light, respectively. For these excitations, the spectrograph was equipped with a holographic grating of 1200 lines/mm. Samples were measured at three different positions, where each of them was exposed to a continuous wave laser. To avoid sample damage, the laser power of 2 mW and 5 mW were used, focused on a 1 and 2 μm diameter spot for 10 s, allowing for the collection of average spectra per sample. Moreover, samples were checked after each measurement. The spectral dependence on apparatus response was considered when correcting the emission spectra. Gaussian model was used to fit the PL spectra of PANI1 and PANI2.

XRD measurements of dried PANI droplets were conducted in transmission Debye–Scherrer mode using a PANalytical Empyrean powder diffractometer (λCu, Kα = 1.54184 Å) equipped with a fixed divergent slit and PIXcel3D detector (30 min, PHD lower level = 4.02 (keV), PHD upper level = 16.10 (keV)). Twenty microliters of PANI suspensions (PANI1 and PANI2) were drop-cast on 1 × 1 cm glass substrates and dried overnight at 40°C. Samples were mounted in a flat sample holder and aligned with the surface holder by dipping it in plasticine. Powder diffraction data were collected using the Bragg–Brentano focusing configuration. One possible error that may occur in the data is not optimized sample height alignment, which may have been caused by immersing the holder in plasticine. This can ultimately lead to a nonlinear shift of 2θ in the diffraction pattern.

SEM images of PANI1 and PANI2 were obtained at 10 kV under 0° (top view) in the regime of secondary electrons (MAIA 3, Tescan). TEM was performed on a Tecnai G2 Spirit Twin 12 (FEI, Czech Republic) at an accelerating voltage of 120 kV, employing bright field imaging. For each sample, 3 μl of the solution was placed on a 300 mesh copper TEM grid covered with an electron-transparent carbon film. The excess solution was quickly removed using filter paper to prevent excessive solute concentration during the drying process. After a 2-min sedimentation period, the grids were left to dry completely at room temperature before observation.

Determination of PANI mass loading was achieved by calculating the PANI composition in a specific volume of suspension. An empty evaporating glass was weighed (m_1), and the specific volume of PANI suspension was drop-cast on an evaporating glass. To maintain a constant weight, the PANI suspension on the glass was dried in an oven (at 40°C). After drying, the evaporating glass with PANI was weighed (m_2). The PANI film was washed with 5 M HCOOH to remove any residual of the initiator left on the glass and then dried again. The final PANI film was weighed (m_3), and the mass loading of PANI was determined by extracting the weight of the evaporating glass. An analytical balance (METTLER TOLEDO, s.r.o.) with 1 μg was used for the weighing measurement.

$$\text{Mass of PANI before washing} = m_2 - m_1 \quad (1)$$

$$\text{Mass of PANI after washing} = m_3 - m_1 \quad (2)$$

$$\text{Mass loading} = m_2 - m_1 \quad (3)$$

$$\text{Determination of PANI mass loading} = \frac{(m_2 - m_1)}{v} \quad (4)$$

where m_1 is the mass of evaporating glass, m_2 is the mass of evaporating glass + dried PANI (before washing),

m_3 is the mass of the evaporating glass + PANI (after washing), and v is the volume of the PANI suspension drop-cast.

Acknowledgments

This work was supported by the Czech Academy of Sciences within the Strategy AV21 framework (VP26-Breakthrough Technology for the Future) and by the MEYS OP JAC project SENDISO (no. CZ.02.01.01/00/22_008/0004596), used the infrastructure of the CzechNanoLab

18626319, 0, Downloaded from https://onlinelibrary.wiley.com/doi/10.1002/pssa.202500433 by Universiteit Hasselt Dienst Financiën, Wiley Online Library on [05/01/2026]. See the Terms and Conditions (https://onlinelibrary.wiley.com/terms-and-conditions) on Wiley Online Library for rules of use; OA articles are governed by the applicable Creative Commons License

(no. LM2023051), and was partially supported by CTU university project no. SGS24/132/OHK4/3T/13 and the Mobility project no. PAN-24-20, between the Czech and Polish Academy of Science. We thank Jan Rohlíček, Ph.D., and R. Jatskivová for the XRD and SEM measurements, respectively.

Open access publishing facilitated by Ceske vysoke uceni technicke v Praze, as part of the Wiley- CzechELib agreement.

Funding

This work was supported by SENDISO (CZ.02.01.01/00/22_008/0004596); CzechNanoLab (LM2023051); CTU university (SGS24/132/OHK4/3T/13); Czech and Polish Academy of Science (PAN-24-20).

Conflicts of Interest

The authors declare no conflicts of interest.

Data Availability Statement

All generated data during this study are available at 10.5281/zenodo.15395015.

References

1. E. Tomšík, S. Boahene, K. A. Dragounová, et al., *Small Methods* 9 (2025): 2401523.

2. M. Winter and R. J. Brodd, *Chemical Reviews* 104 (2004): 4245.

3. S. Yu, N. Yang, S. Liu, and X. Jiang, *Current Opinion in Solid State & Materials Science* 25 (2021): 100922.

4. H. Itoi, S. Hayashi, H. Matsufusa, and Y. Ohzawa, *Chemical Communications* 53 (2017): 3201.

5. A. K. Poddar, S. S. Patel, and H. D. Patel, *Polymers for Advanced Techs* 32 (2021): 4616.

6. U. Rana, S. Mondal, J. Sannigrahi, et al., *Journal of Materials Chemistry C* 2 (2014): 3382.

7. J. Heck, J. Goding, R. Portillo Lara, and R. Green, *Acta Biomaterialia* 139 (2022): 259.

8. J. Kuwabara, W. Tsuchida, S. Guo, Z. Hu, T. Yasuda, and T. Kanbara, *Polymer Chemistry* 10 (2019): 2298.

9. C. Tusy, L. Huang, J. Jin, and J. Xia, *RSC Advances* 4 (2014): 8011.

10. B. Bonillo and T. M. Swager, *Journal of the American Chemical Society* 134 (2012): 18916.

11. R. Ismail, I. Šeděnková, J. Svoboda, M. Lukešová, Z. Walterová, and E. Tomšík, *Journal of Materials Chemistry B* 11 (2023): 1545.

12. B. Aydogan, G. E. Gunbas, A. Durmus, L. Toppare, and Y. Yagci, *Macromolecules* 43 (2010): 101.

13. M. M. Gvozdenović and B. N. Grgur, *Progress in Organic Coatings* 65 (2009): 401.

14. M. Trchová, D. Jasenská, M. Bláha, J. Prokeš, and J. Stejskal, *Spectrochimica Acta Part A: Molecular and Biomolecular Spectroscopy* 235 (2020): 118300.

15. S. Boahene, Š. Potocký, K. Aubrechtová Dragounová, O. Szabó, E. Tomšík, and A. Kromka, *ACS Omega* 10 (2025): 20844.

16. O. Kohut, K. Dragounová, E. Ukraintsev, O. Szabó, A. Kromka, and E. Tomšík, *Vacuum* 171 (2020): 108955.

17. A. B. Rohom, P. U. Londhe, S. K. Mahapatra, S. K. Kulkarni, and N. B. Chaure, *High Performance Polymers* 26 (2014): 641.

18. H. J. Salavagione, C. Sanchís, and E. Morallón, *Journal of Materials Chemistry C* 111 (2007): 12454.

19. J. Sworakowski, *Synthetic Metals* 235 (2018): 125.

20. H. Yoshida, *Journal of Electron Spectroscopy and Related Phenomena* 204 (2015): 116.

21. D. R. T. Zahn, G. N. Gavrila, and M. Gorgoi, *Chemical Physics* 325 (2006): 99.

22. S. Krause, M. B. Casu, A. Schöll, and E. Umbach, *New Journal of Physics* 10 (2008): 085001.

23. S. Lefrant, M. Baibarac, I. Baltog, et al., *Synthetic Metals* 155 (2005): 666.

24. Y. Wu, Y. Ma, X. Shan, et al., *Materials Research Bulletin* 174 (2024): 112711.

25. M. F. Banjar, F. N. Joynal Abedin, A. N. S. Fizal, et al., *Polymers* 15 (2023): 4565.

26. Y. J. Prasutiyo, A. Manaf, and M. A. E. Hafizah, *Journal of Physics: Conference Series* 1442 (2020):012003, https://doi.org/10.1088/1742-6596/1442/1/012003.

27. M. Bláha, F. Marek, Z. Morávková, et al., *ACS Omega* 4 (2019): 7128.

28. P. Y. Wong, S. W. Phang, and A. Baharum, *RSC Advances* 10 (2020): 39693.

29. C. Dhivya, S. A. A. Vandarkuzhali, and N. Radha, *Arabian Journal of Chemistry* 12 (2019): 3785.

30. S. Rafiq, M. A. Lovely, S. R. Mim, M. S. Islam, M. Hasan, and M. M. Billah, *Heliyon* 11 (2025): e42888.

31. Y. He, *Applied Surface Science* 249 (2005): 1.

32. K. A. Ibrahim, *Arabian Journal of Chemistry* 10 (2017): S2668.

33. R. Patil, A. S. Roy, K. R. Anilkumar, and S. Ekhelikar, *Journal of Applied Polymer Science* 121 (2011): 262.

34. S. Golba, M. Popczyk, S. Miga, et al., *Materials* 13 (2020): 5108.

35. D. T. Seshadri and N. V. Bhat, *Journal of Polymer Science. Part B, Polymer Physics* 45 (2007): 1127.

36. L. M. Malec, M. Gryl, and K. M. Stadnicka, *Inorganic Chemistry* 57 (2018): 4340.

37. A. Jumabaev, B. Khudaykulov, I. Doroshenko, H. Hushvaktov, and A. Absanov, *Vibrational Spectroscopy* 122 (2022): 103422.https://doi.org/10.1016/j.vibspec.2022.103422.

38. C. S. Venkateswaran and N. S. Pandya, *Proceedings of the Indian Academy of Sciences* 15 (1942): 390.

39. H. M. Badawi, W. Förner, and S. A. Ali, *Spectrochimica Acta - Part A: Molecular and Biomolecular Spectroscopy* 112 (2013): 388.

40. W. Wang, F. Yang, C. Chen, L. Zhang, Y. Qin, and M. Knez, *Advanced Materials Interfaces* 4 (2017): 1600806.

41. Z. Morávková, M. Trchová, J. Dybal, M. Bláha, and J. Stejskal, *Journal of Applied Polymer Science* 135 (2018): 46728.

42. Z. Morávková and P. Bober, *International Journal of Polymer Science* 2018 (2018): 1.

43. E. Tomšík, O. Kohut, I. Ivanko, M. Pekárek, I. Bieloshapka, and P. Dallas, *The Journal of Physical Chemistry C* 122 (2018): 8022.

44. J. Y. Shimano and A. G. MacDiarmid, *Synthetic Metals* 123 (2001): 251.

45. G. Jhaa, P. D. Pancharatna, and M. M. Balakrishnarajan, *ACS Omega* 8 (2023): 5124.

46. R. A. Marcus, *The Journal of Chemical Physics* 24 (1956): 966.

47. R. A. Marcus and N. Sutin, *Biochimica et Biophysica Acta (BBA) - Reviews on Bioenergetics* 811 (1985): 265.

48. M. Baibarac, I. Baltog, and S. Lefrant, *Journal of Solid State Chemistry* 182 (2009): 827.

49. P. W. Jaschin and K. B. R. Varma, *Journal of Applied Physics* 122 (2017): 083107.

18626319, 0, Downloaded from https://onlinelibrary.wiley.com/doi/10.1002/pssa.202500433 by Universiteit Hasselt Dienst Financiën, Wiley Online Library on [05/01/2026]. See the Terms and Conditions (https://onlinelibrary.wiley.com/terms-and-conditions) on Wiley Online Library for rules of use; OA articles are governed by the applicable Creative Commons License

50. D. D. Borole, U. R. Kapadi, P. P. Mahulikar, and D. G. Hundiwale, *Journal of Applied Polymer Science* 90 (2003): 2634.

51. M. Beygisangchin, S. Abdul Rashid, S. Shafie, A. R. Sadrolhosseini, and H. N. Lim, *Polymers* 13 (2021): 2003.

52. Q. A. Alsulami and A. Rajeh, *Optical Materials* 123 (2022): 111820.

Supporting Information

Additional supporting information can be found online in the Supporting Information section. **Supporting Fig. S1:** SEM images of PANI1 at (a) high and (b) low magnification; PANI2 at (c) high and (d) low magnification. **Supporting Fig. S2:** TEM of (a) PANI1 suspension and (b) PANI2 suspension.

18626319, 0, Downloaded from https://onlinelibrary.wiley.com/doi/10.1002/pssa.202500433 by Universiteit Hasselt Dienst Financiën, Wiley Online Library on [05/01/2026]. See the Terms and Conditions (https://onlinelibrary.wiley.com/terms-and-conditions) on Wiley Online Library for rules of use; OA articles are governed by the applicable Creative Commons License